Confinement in TPE-RX Reversed-Field Pinch

Y. Yagi[1], T. Bolzonella[2], A. Canton[2], K. Hayase[1], Y. Hirano[1], S. Kiyama[1], H. Koguchi[1], Y. Maejima[1], J-A. Malmberg[3], H. Sakakita[1], Y. Sato[1], S. Sekine[1], T. Shimada[1], K. Sugisaki[1]

1) Electrotechnical Laboratory, Tsukuba 305-8568 Japan
2) Consorzio RFX, Padua 35127 Italy
3) Royal Institute of Technology, Stockholm 100 44 Sweden

e-mail contact of the main author: yagi@etl.go.jp

Abstract. Characteristics of the confinement properties of a reversed field pinch (RFP), the TPE-RX (R/a = 1.72/0.45 m, R and a are major and minor radii), are presented for the plasma current, I_p of 0.2-0.4 MA. TPE-RX has been operational since 1998, and I_p = 0.5 MA and duration time of up to 0.1 s have been obtained separately. It is found that I_p/N (= 12 x 10^{-14} Am, N is the line density) is higher than those of other RFPs and poloidal beta, β_p, and energy confinement time, τ_E, are 5-10% and 0.5-1 ms, respectively, which are comparable with those of other RFPs of comparable sizes (RFX and MST). Pulsed poloidal current drive has recently been tested and the result has shown a twofold improvement of β_p and τ_E. The improvement is discussed in terms of the dynamic trajectories in the F-Θ plane, where F and Θ are reversal and pinch parameters, respectively. The global confinement properties are compared between the locked and nonlocked discharges, which yields a better understanding of the mode-locking phenomena in RFP plasmas.

1. Introduction

The reversed field pinch (RFP) [1] has many merits as a potential reactor, such as its relatively high beta value with normal-conducting toroidal coils and its ability to achieve a reactor relevant condition with joule heating (without using additional heatings), which can enable a simple toroidal confinement system. One of the important issues in RFP studies is how the confinement properties as well as the magnetohydrodynamic (MHD) activities, which are closely related to the dynamo activities [2], behave up to the reactor condition. An understanding of the underlying physics of the energy and particle transport, in addition to experiments on controlling the MHD activity, are of crucial importance. This paper presents the most recent database of an RFP, TPE-RX [3] at the Electrotechnical Laboratory, in terms of the global confinement properties at the plasma current, I_p = 0.2-0.4 MA with an improved confinement mode, and the MHD activities exhibited in the locked mode.

TPE-RX is a large RFP machine (R/a = 1.72/0.45 m, R and a are the major and minor radii, respectively) and is characterized by a close-fitting (b/a = 1.08, b being the minor radius of the innermost shell) conductive shell with equilibrium control by means of the DC external field with the aid of a pulsed poloidal coil inside the thick shell which assists gas breakdown. The vacuum vessel is made of 316L stainless steel with fixed molybdenum limiters. Goals of the TPE-RX are to optimize and to understand the confinement properties of RFP plasmas up to the designed maximum plasma current (I_p) of 1 MA. The maximum I_p and pulse duration time, τ_d, of 0.48 MA and 0.1 s have been independently attained. The maximum I_p is limited by the total energy of the present capacitor bank system.

2. Global Confinement Properties

The TPE-RX has been routinely operational since the start of physics experiments in 1998, and the performance observed in the basic waveforms has become stable to the situation reported in Ref. [4]. A single-point Thomson scattering system, single-chord neutral particle energy analyzer (NPA) and a dual-chord interferometer system have recently been developed for the TPE-RX, and electron and ion temperature and electron density measurements are now possible. Consequently, the estimation of the global confinement time has become possible, for the first time, in the TPE-RX. The experimental results shown here are those obtained without using an active density controlling scheme such as gas puffing or pellet injection. The electron density increases linearly with I_p. Pinch parameter Θ (= B_{pa} /<B_t>, where B_{pa} and <B_t> are the poloidal magnetic field on the plasma surface and the volume-averaged toroidal magnetic field,

respectively), was kept constant at 1.5. Temporal evolution of the central electron temperature, T_{e0}, and ion temperature, T_i, and the line-averaged electron density, n_{el}, were obtained. After the current-rising phase, T_{e0} and n_{el} had the maximum values at the center of the current flat top (t = 31 ms), and the observation time for the I_p-scan was fixed at t = 31 ms. Then, I_p was scanned from 0.2 MA to 0.4 MA. Equilibrium control was passively maintained by the conductive shell. The maximum shift of the center of the last closed flux surface (LCFS) is estimated to be 2 mm (0.4% of a) at I_p = 0.4 MA.

2.1 Behaviour of Electron Density

From the measurement of the line-averaged electron density, n_{el}, it is found that the I/N value of the normal RFP discharges in TPE-RX is 12 x 10^{-14} Am on average [5], which is higher than those of other RFP plasmas, where $I = I_p$ and N (= $\pi a^2 \langle n_e \rangle$) is the line density and $\langle n_e \rangle$ is the volume-averaged electron density. For example, I/N = 2-6 x 10^{-14} Am in RFX, 4-12 x 10^{-14} Am in MST and 2-15 x 10^{-14} Am in T2. Figure 1(a) shows n_{el} versus I_p. The result shows that I/N ranges from 8 to 20 x 10^{-14} Am. Note here that the values of n_{el} are converted from n_{e0} of Thomson scattering so that the average proportionality to I_p holds. This is to enable a consistent data analysis when n_{el} from the interferometer is not available. This high I/N value, however, is the same as those of previous TPE machines of different sizes, TPE-1RM15 and TPE-1RM20 [6], which were made of the same materials as those of TPE-RX for the vacuum vessel (316L stainless steel) and limiters (molybdenum). This result indicates that the source term, S_{el}, of the electrons, under the steady-state condition, should scale as $S_{el} \sim I_p / (\tau_p a^2)$, where τ_p is the particle confinement time. Thus, TPE-RX provides confinement characteristics of RFP plasmas in the high I/N region. The physical meaning of the high I/N value is discussed in 2.3.

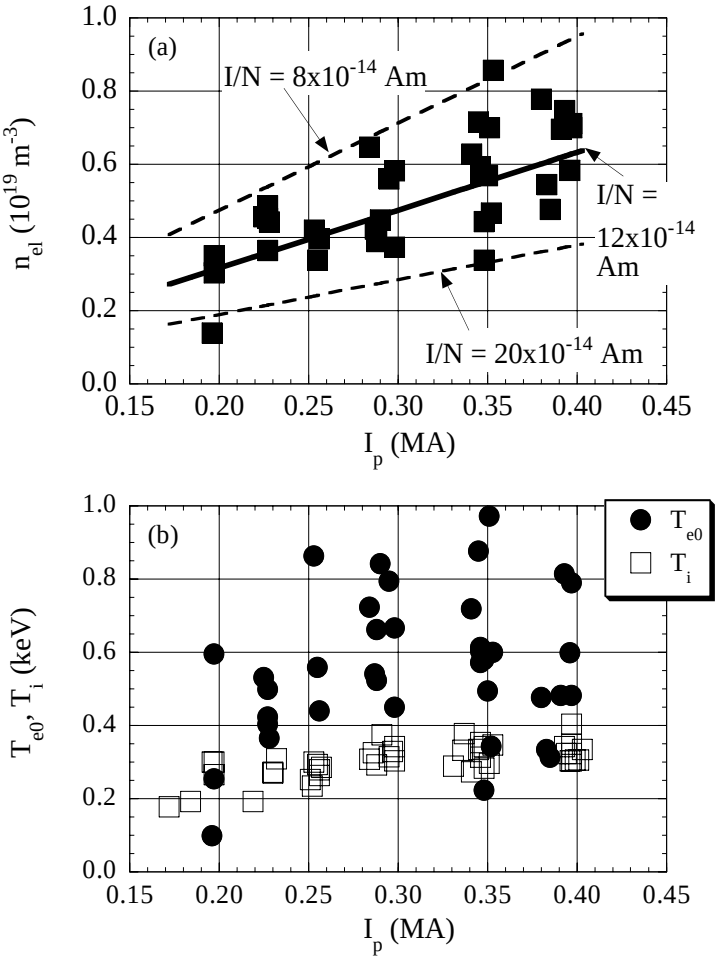

Fig. 1 (a) n_{el} versus I_p with the range of I/N, and (b) T_{e0} versus I_p.

Information on the spatial profile of n_{el} has recently been obtained through two-chord simultaneous measurement at r = 0 and 31 cm at I_p = 0.25 MA. The result shows that the ratio of n_{el} at r = 31 cm and 0 is 0.75 +- 0.10 at t = 20-60 ms. The value indicates that the electron density profile is broad, and the power x ranges from 3.4 to 8.1 with the most probable center being at x = 5.1 for the assumed profile of $1-(r/a)^x$.

2.2 Electron and Ion Temperatures

Energy distribution functions of electrons and ions were examined and it was confirmed that both can be expressed by normal Maxwellian distribution functions up to the observed energy range of 3 keV.

Figure 1(b) shows T_{e0} and T_i versus I_p. Both T_{e0} and T_i increase with I_p, but T_{e0} becomes saturated at I_p = 300 kA, while T_i continues to increase offset-linearly to I_p. The ratio T_i/T_{e0} ranges from 0.5 to unity depending on I_p. It is estimated that anomalous ion heating should be operational in TPE-RX, but to a lesser extent than in the previous machine, TPE-1RM20.

2.3 β_p and τ_E

Figure 2 shows the poloidal beta, β_p, and energy confinement time, τ_E, which have been estimated from the values shown in Fig. 1. We assumed $T_{i0} = T_i$, $n_i = n_e$ and a parabolic profile for the pressure, where T_{i0} is the central ion temperature and T_i is the ion temperature obtained from the NPA. The assumption of $n_e = n_i$ can cause an overestimation of the pressure by 10-40 % for Z_{eff} = 4. This overestimation is comparable to the shot-by-shot deviation of T_{e0}, T_i and n_{el}. Figure 2 shows that β_p and τ_E range from 5% to 10%, and from 0.5 ms to 1.0 ms, respectively, for the scanned range of I_p. It is seen that τ_E has a weak dependence on I_p. This is due partly to the increase of the loop voltage with I_p [4] and partly to the degradation of T_{e0} at I_p > 300 kA, as seen in Fig. 1(b). This point is discussed in more detail below.

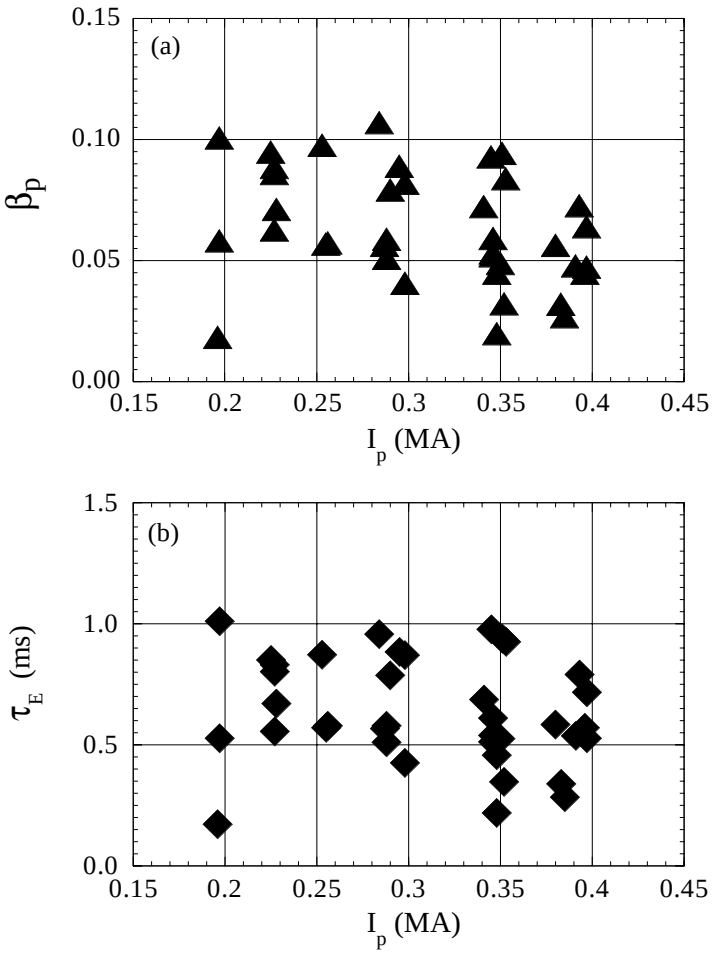

Fig. 2 (a) β_p versus I_p, (b) τ_E versus I_p.

2.4 Discussions on the Global Confinement

In RFPs, experimentally obtained values of τ_E are often compared with the theoretical scalings. The best theoretical scaling for τ_E is that determined by the g-mode [7]. According to this scaling, τ_E^{CT} (s) = $51.6\, a^2\, h^{-1} Z^{*-1}\, \beta_p^{5/2}\, (I/N)[10^{-14}\mathrm{Am}]^{3/2}\, I_p[\mathrm{MA}]^{3/2}$, where h is the helical factor, Z^* is Z_{eff} including anomaly effects [8], and the proportional coefficient is obtained from the confinement properties in TPE-1RM20 [9]. We calculate the ratio $\gamma = (\tau_E/\tau_E^{CT})^{-1}$, which is essentially $Z^*_{\mathrm{TPE\text{-}RX}}/Z^*_{\mathrm{TPE\text{-}1RM20}}$ if the same values for h (= 10) and Z^*(= 4) are used. The result is plotted in Fig. 3 as a function of I_p. Figure 3 shows that γ increases slightly with I_p. Note that γ is the target value for the improvement factor of the

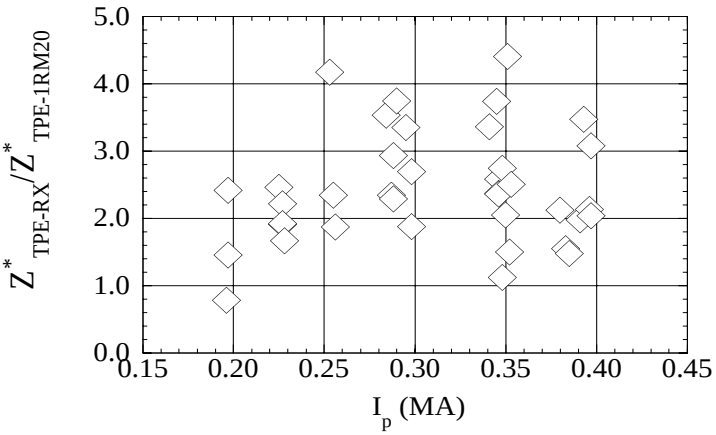

Fig. 3 Comparison of Z between TPE-RX and TPE-1RM20 estimated from the constant β_p scaling*

present confinement of TPE-RX with respect to that of TPE-1RM20. Also note that the values of β_p in TPE-RX is 70-80% of that in TPE-1RM20, so that the constant β_p scaling does not hold in these two machines. Empirical scaling studies including as much database as possible are necessary to conclude the applicability of the constant β_p scaling.

It was shown that *I/N* in TPE-RX is higher than in other existing RFPs. The underlining physics connected to *I/N* in terms of the energy transport, however, are not yet well understood. It can be readily shown that *(I/N)/e* is electron drift velocity, v_d. In terms of nondimensional parameters, *I/N* is closely related to the electron streaming parameter ξ ($= v_d/v_{th}$) and electron mean-free-path normalized by *a*, λ_{mfp}/a. Figure 4 shows ξ and λ_{mfp}/a as functions of *I/N*. It is of interest to note that λ_{mfp}/a is as large as the designed value of an RFP reactor [10]. Convective loss of energy along stochastic magnetic field lines in the core plasma can have a significant influence under high values of λ_{mfp}/a. How the magnetic fluctuation amplitude scales with the Ludquist number, *S*, is another important issue of RFP plasmas in predicting how the magnetic stochasticity behaves under reactor relevant plasma conditions. A recent study [11] shows that b_{rms}/B_{pa} scales as $S^{-0.18}$ which is similar to MST [12], RFX [13] and T2 [11].

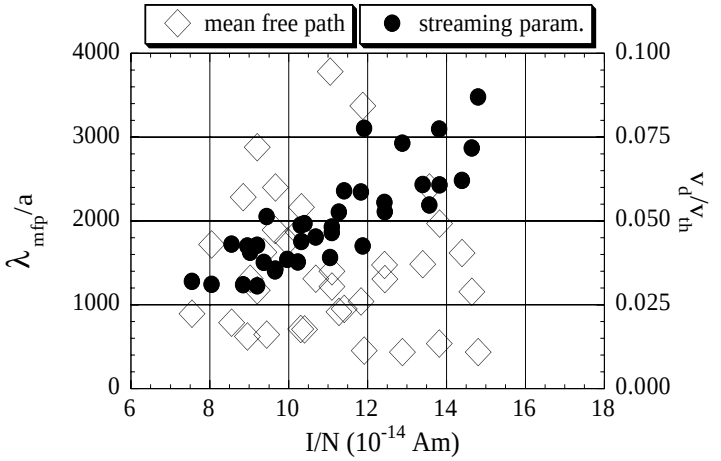

Fig.4 λmfp/a and the streaming parameter are plotted versus I/N.

In order to achieve further improvement of confinement in TPE-RX, we plan to separate the methods for the improvement into machine- or operation-dependent causes and intrinsic causes for the conventional RFP plasmas. One direction along the former lines is to mitigate the plasma wall interaction at high I_p, particularly at I_p > 300 kA, to optimize the equilibrium control, and to increase the density in order to lower *I/N*. Alternative direction related to the latter is to try an improved confinement mode, or more directly, to control the current profile for better stability while sustaining the RFP configuration by some external means.

3. Pulsed Poloidal Current Drive

Several types of improved confinement modes have recently been observed in many RFP machines. Pulsed poloidal current drive (PPCD) is one of them. It was originally achieved at MST at U. Wisconsin [14]. In a recent PPCD experiment at MST, they achieved a fivefold improvement of the energy confinement time [15]. The original idea of the PPCD is to drive the poloidal current inductively, without relying on dynamo activities. Indeed, the magnetic fluctuation amplitude was reduced during the PPCD and the stored energy, and hence τ_E, was improved [14,15].

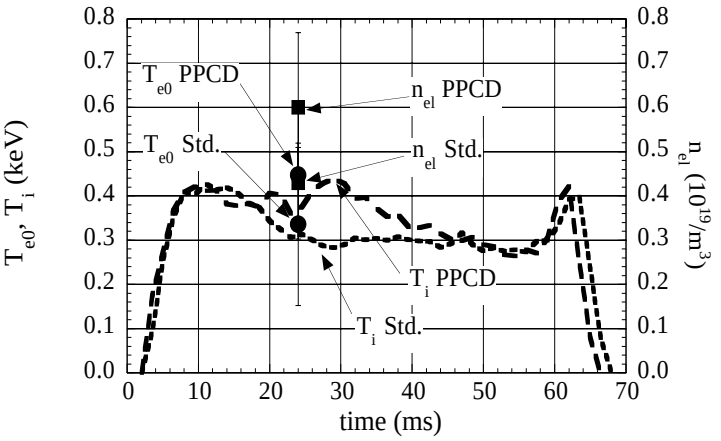

Fig. 5 Temporal evolutions of T_{e0}, n_{el}, and T_i during PPCD in TPE-RX.

3.1 PPCD Experiment in TPE-RX

It is possible to apply one-pulse PPCD in TPE-RX. The toroidal reversal bank is triggered after the current-rising phase (t ~ 20 ms). Then, F is transiently deepened, and Θ increases accordingly. The penetration time of the m=0 perturbation into the vacuum vessel is 2 ms. It was observed that the soft X-ray signal rises sharply within 4 ms after triggering the PPCD ($t = t_{peak}$) and subsequently it often shows a crash event. Occasionally, the intensity of the soft X-rays is sustained at the level of the peak when such a crash event is spontaneously avoided. Figure 5 shows the shot-averaged temporal evolution of T_{e0}, T_i and n_{el} during the PPCD at I_p = 300 kA. Both T_{e0} and n_{el} have peaks at $t = t_{peak}$ and T_i later has a broad peak at t = 30 ms. At $t = t_{peak}$ it is estimated that both β_p and τ_E have increased by a factor of two.

3.2 Numerical Simulation and Interpretaion

Another improved mode, which was observed in TPE-1RM20, was the high-Θ mode (IHTM) [16]. The IHTM is the mode where a large-sawtooth crash spontaneously disappears at high Θ (~2), and both β_p and τ_E increase by a factor of two. The equilibrium configuration expressed by F and Θ changes during the PPCD. In this sense, PPCD is an in-shot Θ-scan experiment. We attempted to elucidate how much the transient nature of the PPCD is related to the improvement. We compared the global confinement properties between the PPCD discharges and the shot-by-shot Θ-scan discharges. First, it should be noted here that since the maximum Θ value was limited to 1.8 due to the limitation of the toroidal bank system, it has not yet been possible to conclude if the IHTM is obtainable in TPE-RX or not. Nevertheless, we can compare the in-shot Θ-scan and the shot-by-shot Θ-scan within the attainable range of (F-Θ).

Figure 6 shows the trajectories of the shot-averaged PPCD discharges and four cases of the shot-by-shot Θ-scan discharges. The trajectory of the PPCD follows a line of a deeper F than those for the shot-by-shot Θ-scan discharges. If the PPCD is operated keeping $\tau_{PPCD} < \tau_R(0)$, then B_{tw} deepens while $B_t(0)$ remains almost unchanged, where $\tau_{PPCD} = (1/B_{tw}\ (dB_{tw}/dt))^{-1}$ and $\tau_R(0)$ is the resistive diffusion time at the plasma centre. In the F-Θ plane, the normal trajectory follows a line of $(1-F)/\Theta = (\langle B_t \rangle - B_{tw}) / B_{pa} = \langle B_t - B_{tw} \rangle / B_{pa}$ = constant [17]. Thus, it is understood that the F-Θ trajectory follows a deeper line in the case of the PPCD. Recently, we have performed a numerical simulation of the nonlinear evolution of the magnetic fluctuation amplitudes during the PPCD, changing the ratio of $\tau_{PPCD}/\tau_R(0)$. The result is shown in Fig. 7. It is shown that the reduction of the magnetic fluctuation amplitude becomes larger as $\tau_{PPCD}/\tau_R(0)$ becomes smaller. This indicates that the PPCD is a means of boosting the operating point in the F-Θ plane to a more stable position. This change is

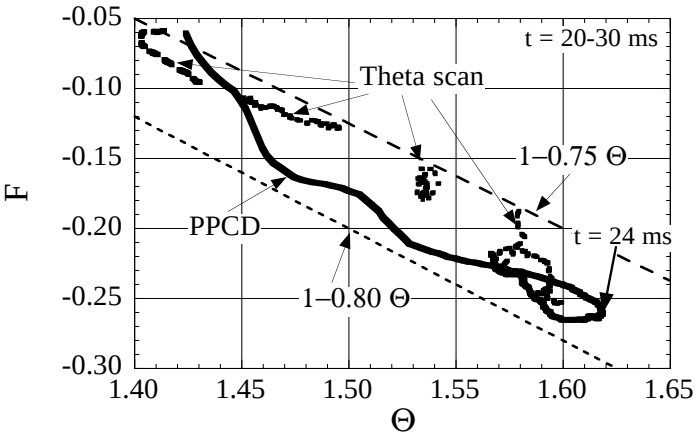

Fig. 6 Trajectories in the F-Θ plane for PPCD and Θ scans.

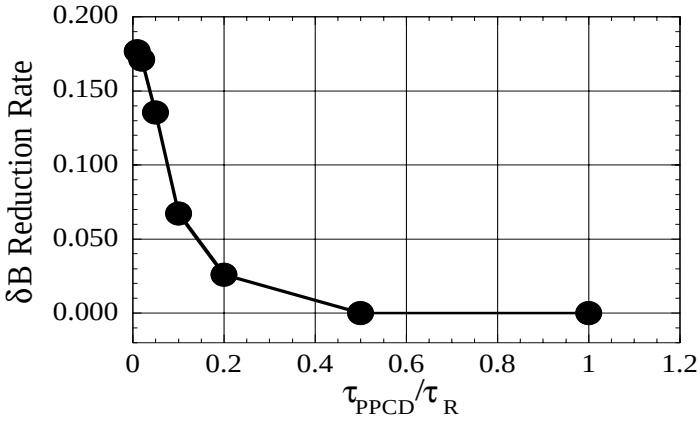

Fig. 7 The reduction rate of the magnetic fluctuation amplitude is numerically simulated as a function of τ_{PPCD}/τ_R.

achieved transiently in the case of PPCD. However, it would be achievable for the steady-state operation by tailoring the current profile by means of an RF technique, for example.

4. Phase and Wall Locking

In TPE-RX, the phase- and wall-locked structure, which is called LM hereafter, has been observed [18]. The locked mode is commonly observed in many RFPs. Recently, active rotation of the LM has been successfully conducted in RFX [19] so that the plasma wall interaction (PWI) caused by the LM can be alleviated. It is also found that in TPE-RX there are nonlocked discharges (NonLM) where the prominent phase-locked structure disappears. It is also of great interest to compare the global confinement properties between the LM and NonLM. In this section, we present the recent observation of the LM in TPE-RX using the B_t-array signal, a comparison of the growth of the mode amplitude with the theoretical threshold, and a comparison of the global confinement properties between the LM and NonLM discharges.

4.1 Typical Locked Mode and Its Threshold

A clear LM structure of the magnetic field fluctuation was observed by using the B_r pick-up coil arrays [18]. The B_r component is suitable for reconstructing the shift of the last closed flux surface (LCFS). However, the B_r signals do not clearly indicate whether the modes rotate before they lock to the wall, because of the relatively small B_r signal near the conductive shell. Recently, we measured the B_t-array signal and a slow rotation of the mode prior to the wall-locking was clearly observed. Figure 8 shows the temporal evolution (t = 5-30 ms) of the toroidal profile of the m = 1 (odd) component of the B_t signal in a typical locked-mode discharge at I_p = 250 kA. Figure 8 shows that a phase-locked structure (spatially localized enhanced magnetic amplitude) toroidally propagates during the current-rising phase (t = 5-15 ms) in the anti-I_p direction. The rotation stops at t = 17 ms at the toroidal angle ϕ = 130 degrees, and this wall-locked structure persists throughout the discharge. In the case of NonLM discharges, the propagation speed of the modes is faster, and the mode amplitudes are lower than in the LM case, but the modes eventually wall-lock in the current flat-top phase. Note that the NonLM here is the state where the phase-locked structure becomes much less conspicuous than the LM.

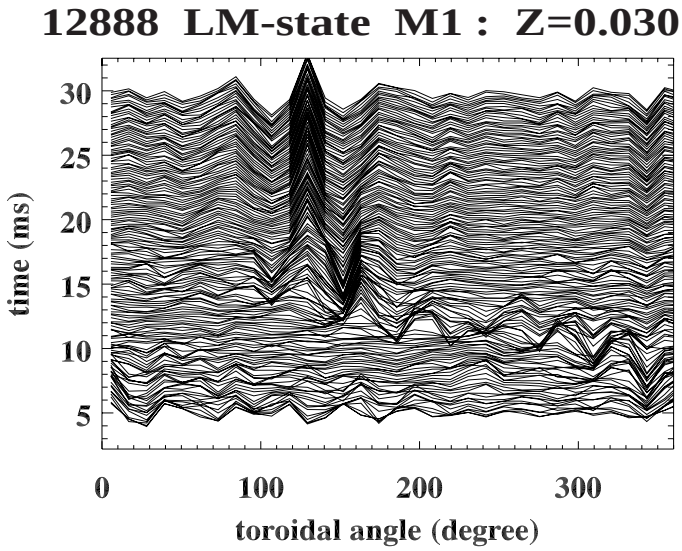

Fig. 8 Wall locking of the phase-locked structure.

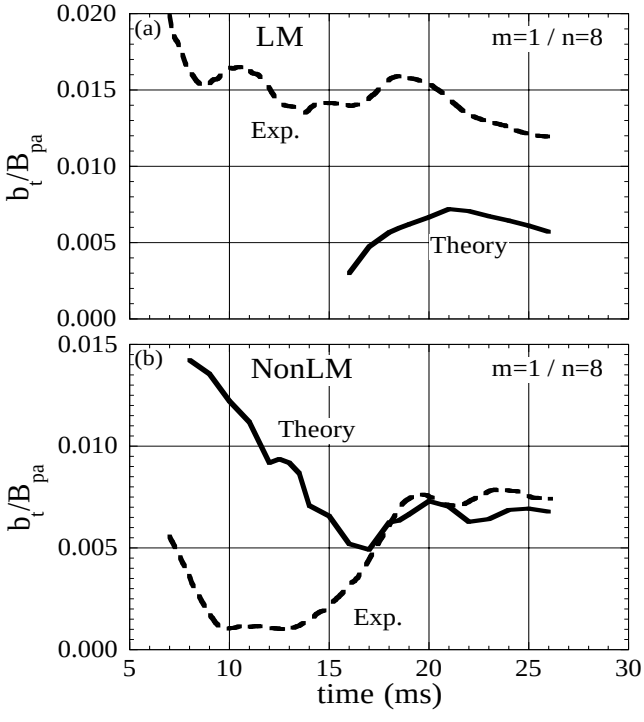

Fig.9 Comparison of the wall-locking threshold

The mode spectrum and phase velocity are analyzed for the LM and NonLM discharges, and the mode amplitudes are compared with the theoretically predicted level [20]. The theory predicts that the mode wall-locks due to the dragging torque between the island of the mode and the eddy current induced in the vessel. The temporal evolution of the global confinement properties measured in the LM and NonLM discharges (see Sec. 4.2) is used in the calculation. Figure 9 shows a comparison of the shot-averaged mode amplitudes of the $m = 1/n = 8$ mode and the theoretically predicted levels required for the mode to wall-lock for the LM and NonLM cases. It is seen that in the LM case, the mode amplitude always exceeds the theoretical threshold. In the NonLM case, however, it is initially well below the threshold, then gradually approaches the threshold and becomes comparable to the threshold at $t = 17$ ms when the wall-locking actually occurs.

Comparison of the phase-locking threshold and the mode amplitude is more straightforward for explaining why there are LM and NonLM discharges in TPE-RX. However, in this case, a quantitative comparison is difficult. Since the dependence of the theoretical threshold on the physics quantities is qualitatively similar [21] to that of the wall-locking threshold, it is sufficient to state here that the NonLM appears in TPE-RX because T_e is higher during the current rising phase than those in the LM discharges (see 4.2).

4.2 Comparison of the Global Confinement Properties

A severe PWI has been observed in TPE-RX [22] where a peaking of the thermal heat load has been observed. The effect of the LM on the global confinement properties has been a crucial issue for the RFP plasma. In TPE-RX, it is possible to compare the global confinement properties between the LM and NonLM discharges. We conducted a series of experiments at I_p = 250 kA, $\Theta = 1.5$ and the filling pressure of deuterium p_{D2} = 0.7 mTorr and 0.3 mTorr, for the LM and NonLM discharges.

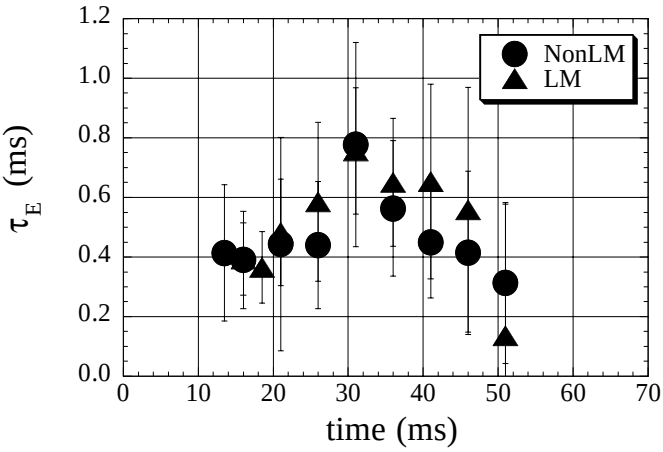

Fig. 10 Global confinement properties of LM and NonLM.

The results are plotted in Fig. 10 against τ_E. Figure 10 shows that τ_E does not differ significantly between the LM and NonLM discharges. Differences are seen in T_{e0} and n_{el} during the current-rising phase. Because of the higher p_{D2} in the LM discharges, n_{el} is higher than that in the NonLM discharges. Note, however, that n_{el} during the current flat-top phase does not differ very much, indicating that the electron density is limited by the transport rather than the source term. On the other hand, T_{e0} is higher for NonLM than for LM. This helps to increase the intrinsic plasma velocity, and eventually, to lower the theoretical threshold [20,21] for both wall and phase locking, as described in Sec. 4.2.

5. Conclusion

Three major topics of recent research on a large RFP, TPE-RX, were reported. First, the global confinement properties at I_p = 0.2-0.4 MA were measured for the first time since the start of the physics experiments in 1998. The range of I/N was found to be higher (12×10^{-14} Am) than in other existing RFPs, but comparable to those of previous TPE machines. The measured τ_E ranged from 0.5 to 1.0 ms. Possible means of improvement were discussed. Second, an improved confinement mode, PPCD [14,15], was tested. The result shows a twofold improvement of β_p and τ_E, and a further deepening of the F appears promising. Third, the understanding of the mode-locking phenomena has progressed since the initial observations

[18]. At relatively low I_p (= 0.25 MA), the LM discharge was found to have comparable τ_E during the current flat-top phase, but is different in terms of T_{e0} and n_{el} during the current-rising phase, compared to those of the NonLM discharge. This difference has the important effect of causing a difference in the intrinsic plasma velocity and the threshold for both wall and phase locking [20,21]. The existence of the LM may not be a bottleneck of the energy transport, though severe PWI should be avoided, as was done in RFX [19]. The global confinement in TPE-RX can be improved by a method in line with the PPCD which suppresses the intrinsic MHD activities while sustaining the RFP configuration.

Acknowledgment

The authors are grateful to Dr. Y. Owadano for discussions and encouragement to pursue this work. The authors are grateful to Dr. S. Martini, Dr. P. Zanca, and Dr. P. L. Brunsell, particularly for the collaborative work on the locked-mode issue and for the use of equipment for the experiments on TPE-RX. The authors are also grateful to Dr. H. Ashida for the development of the MHD code used in the numerical simulations presented in the paper. One of the authors (J-A. M.) was supported by a grant from ABB (Area Brown Boveri) administrated by the Sweden-Japan foundation, during her stay at the Electrotechnical Laboratory. This work is financially supported by the Japanese Science and Technology Agency.

References

[1] BODIN, H. A. B. and NEWTON, A. A., Nucl. Fusion **20** (1980) 1255.
[2] MOFFAT, H. K., in *Magnetic Field Generation in Electrically Conducting Fluids* (Cambridge University Press, 1978).
[3] YAGI, Y., et al., Fusion Eng. and Design **45** (1999) 409.
[4] YAGI, Y., et al., Plasma Phys. Controlled Fusion **41** (1999) 255.
[5] HIRANO Y., et al., in Fusion Energy (Proc. 17th Int. Conf., Yokohama, 1998) Vol. 1 (2000) 375.
[6] YAGI, Y., et al., Nucl. Fusion **40** (2000) 223.
[7] CONNOR, J. W. and TAYLOR, J. B., Phys. Fluids **27** (1984) 2676.
[8] YAGI, Y. et al., *Proc. Int. School of Plasma Physics, Course and Workshop on Physics of Mirrors, Reversed Field Pinches and Compact Tori*, Varenna, Italy, 1990, (ed. by S. Ortolani and E. Sindoni, Societa Italiana Di Fisica, Bologna, 1991), p. 1029.
[9] YAGI, Y., HIRANO, Y., MAEJIMA, Y., SHIMADA, T., and HIROTA, I., Trans. Fusion Tech. **27** (1995) 301.
[10] KRAKOWSKI, R. A., Fusion Technology **20** (1991) 121.
[11] MALMBERG, J-A., BRUNSELL, P., YAGI, Y., and KOGUCHI, H., *to be published in* Phys. of Plasmas.
[12] FIKSEL, G., et al., Fusion Energy, Proc. 17th Conf., Yokohama, 1998, (IAEA Vienna), Vol. 1 (1999) p. 383.
[13] INTRAVIATA, A., et al., Phys. Rev. Lett., **83** (1999) 5499.
[14] SARFF, J., et al., Phys. Rev. Lett., **72** (1994) 3670.
[15] SARFF, J., LANIER, N. E., PRAGER, S. C., and STONEKING, M. R., Phys. Rev. Lett., **78** (1997) 62.
[16] HIRANO, Y., MAEJIMA, Y., SHIMADA, T., HIROTA, I., and YAGI, Y., Nucl. Fusion, **36** (1996) 721.
[17] MAEJIMA, Y. and ASHIDA, H., Proc. 25th EPS, Prague, 1997, ECA Vol. 21A Part I, p. 1784.
[18] YAGI, Y., et al., Phys. of Plasmas **6** (1999) 3824.
[19] BARTIROMO, R., Phys. Rev, Lett., **83** (1999) 1779.
[20] FITZPATRICK, R., GUO, S. C., and DEN HARTOG, D. J., Phys. Plasmas, **6** (1999) 3878.
[21] FITZPATRICK, Phys. Plasmas, **6** (1999) 1168.
[22] YAGI, Y., SEKINE, S., BOLZONELLA, T., SAKAKITA, S., and KOGUCHI, H., *to be published in* J. of Nucl. Mat (*Proc. of 14th PSI, Rosenheim, 2000*).